mathematics

MDPI

Article

Dynamic Behavior and Bifurcation Analysis of a Modified Reduced Lorenz Model

Mohammed O. Al-Kaff [1,2,*], Ghada AlNemer [3,*], Hamdy A. El-Metwally [1], Abd-Elalim A. Elsadany [4,5] and Elmetwally M. Elabbasy [1]

1 Department of Mathematics, Faculty of Science, Mansoura University, Mansoura 35516, Egypt; helmetwally@mans.edu.eg (H.A.E.-M.)
2 Department of Mathematics, College of Education, Seiyun University, Seiyun, Yemen
3 Department of Mathematical Sciences, College of Sciences, Princess Nourah Bint Abdulrahman University, Riyadh 11671, Saudi Arabia
4 Mathematics Department, College of Science and Humanities Studies Al-Kharj, Prince Sattam Bin Abdulaziz University, Al-Kharj 11942, Saudi Arabia; aelsadany1@yahoo.com
5 Basic Science Department, Faculty of Computers and Informatics, Suez Canal University, Ismailia 41522, Egypt
* Correspondence: abohassien246@seiyunu.edu.ye (M.O.A.-K.); gnnemer@pnu.edu.sa (G.A.)

Abstract: This study introduces a newly modified Lorenz model capable of demonstrating bifurcation within a specified range of parameters. The model demonstrates various bifurcation behaviors, which are depicted as distinct structures in the diagram. The study aims to discover and analyze the existence and stability of fixed points in the model. To achieve this, the center manifold theorem and bifurcation theory are employed to identify the requirements for pitchfork bifurcation, period-doubling bifurcation, and Neimark–Sacker bifurcation. In addition to theoretical findings, numerical simulations, including bifurcation diagrams, phase pictures, and maximum Lyapunov exponents, showcase the nuanced, complex, and diverse dynamics. Finally, the study applies the Ott–Grebogi–Yorke (OGY) method to control the chaos observed in the reduced modified Lorenz model.

Keywords: Lorenz model; pitchfork bifurcation; period-doubling; Neimark–Sacker bifurcation; chaos

MSC: 39A10; 39A23; 39A28; 39A30; 39A33

Citation: Al-Kaff, M.O.; AlNemer, G.; El-Metwally, H.A.; Elsadany, A.-E.A.; Elabbasy, E.M. Dynamic Behavior and Bifurcation Analysis of a Modified Reduced Lorenz Model. *Mathematics* **2024**, *12*, 1354. https://doi.org/10.3390/math12091354

Academic Editors: Inna Samuilik, Felix Sadyrbaev and Alicia Cordero

Received: 25 February 2024
Revised: 12 April 2024
Accepted: 23 April 2024
Published: 29 April 2024

1. Introduction

The nonlinear dynamical model is well-known for its applications in various fields, such as population growth, economics, physics, mechanics, technology, and others. One of the most important discoveries in modern science is the identification of irregular vibrations in addition to periodic and nearly periodic vibrations. A comprehensive study of nonlinear scientific theory and its applications can significantly alter one's perspective on various nonlinear phenomena and laws, along with their profound implications across a wide range of applications. Bifurcation theory, chaos theory, and singularity theory have all gained increasing importance in the field of nonlinear science over the past few decades. These theories are rapidly advancing in their applications to physics, mathematics, and numerous technical fields worldwide. Chaotic mappings have witnessed extensive applications in computer sciences over the past few decades, particularly in domains such as digital image processing [1] and communication systems [2]. Notable examples of general chaotic mappings include logistic mapping [3], Henon mapping [4], Lorenz mapping [5], and others. Numerous scholars have made significant contributions to understanding the dynamic properties of these chaotic mappings. Annaby et al. [6] presented an image encryption algorithm that combined Henon chaos and logistic systems. Experimental results demonstrated superior security against statistical attacks and differential attacks compared to the classical encryption algorithm and the improved encryption algorithm. Furthermore, Mliki et al. [7] introduced new chaotic maps with applications in stochastic processes, while Ramadoss et al. [8] recently investigated the behaviors of a one-dimensional chaotic map comprising two sine terms. Overall, these references highlight the wide-ranging applications and significant contributions made in the field of chaotic mappings, underscoring their relevance and advancements in various areas of research.

Lorenz's simplified model [9] involves a pair of coupled differential equations that are estimated. The subsequent section provides the definition of the reduced Lorenz model:

$$\begin{cases} \varkappa_{n+1} = \varkappa_n + \alpha t \varkappa_n - t \varkappa_n \gamma_n, \\ \gamma_{n+1} = \gamma_n - t\gamma_n + t\varkappa_n^2. \end{cases} \tag{1}$$

The integral step size is given by t, which originated from the simple forward Euler integral between two paired nonlinear differential equations as follows:

$$\begin{cases} \dfrac{d\varkappa}{dt} = \alpha\varkappa - \varkappa\gamma, \\ \dfrac{d\gamma}{dt} = \varkappa^2 - \gamma. \end{cases} \tag{2}$$

This study will be based mostly on the Lorenz reduction model [9–11], which has been modified from the Lorenz reduction model as follows:

$$\begin{cases} \dfrac{d\varkappa}{dt} = \alpha\varkappa(1-\varkappa) - \varkappa\gamma, \\ \dfrac{d\gamma}{dt} = \varkappa^2 - \gamma, \end{cases} \tag{3}$$

where a non-negative, from (3), we obtain the following model using the Euler technique:

$$\begin{cases} \varkappa_{n+1} = (1+\alpha h)\varkappa_n - h\varkappa_n\gamma_n - \alpha h \varkappa_n^2, \\ \gamma_{n+1} = (1-h)\gamma_n + h\varkappa_n^2. \end{cases} \tag{4}$$

Numerical analysis of the model (1) was presented in [9,10], demonstrating a richer collection of dynamical patterns compared to the continuous case. Elabbasy et al. [11] provided both a theoretical examination and a numerical analysis of the bifurcation phenomenon in the model (1). Zhao et al. [12] investigated the stability and bifurcation of a discrete predator-prey model featuring a modified Holling–Tanner functional response. Al-Kaff et al. [13] performed bifurcation analysis and chaos control in a discrete predator-prey system, focusing on understanding the bifurcation behavior and developing control methods. Additionally, Zhang et al. [14] explored transcritical and period-doubling bifurcations in a discrete predator-prey model with a strong Allee effect. For further papers on nonlinear dynamical systems and models, readers can refer to [15–19]. The step size used for integration is denoted by h. We have discovered that for the reduced modified Lorenz model (4), a smaller integrated step size can demonstrate the model's local stability. However, using a larger integrated step size may result in model instability, leading to the emergence of complex and diverse dynamics. This highlights the importance of the model (4) in exploring the concepts of computational bifurcation and chaos. There are several applications in which chaos can be used. Moreover, a chaotic dynamic model is not only vital and valuable, but it may also bring a new approach or model that may help people understand mathematics. A recent innovation in the field of encryption research is the use of chaotic dynamics for information security. Two-dimensional and three-dimensional discretized chaotic maps were presented as the foundation for a new encryption [20,21]. Zhu et al. [22] demonstrated the superiority of constructing chaotic maps based on encryption techniques and have established that chaotic maps contain significant properties connected to the essential criteria of traditional encryption algorithms in many respects.

This model (4) had not been studied before, as we added the term $\alpha\varkappa^2$ to the model (2) until we had a logistic function of the model (3), which played an important role in our findings. We presented a numerical and theoretical analysis of the bifurcation and chaos for the model (4), which revealed a much richer and more complex structure with some interesting results.

Motivated by the aforementioned works, this study focuses on examining the nonlinear dynamical behavior of (4). The paper is organized as follows: In Section 2, we investigate the existence and stability of the fixed points in the model. Section 3 provides a detailed discussion on the pitchfork bifurcation, Period-doubling bifurcation (PB), and Neimark–Sacker bifurcation (NB). In Section 4, we employ a chaos control strategy to effectively manage the chaotic behavior displayed by the model (4). Finally, numerical simulations are conducted to further elucidate the main results obtained in the study.

2. The Existence and Stability of the Fixed Points Are Examined

In this section, we delve into the qualitative properties of the fixed points within the model (4), as well as the conditions for asymptotic fixed point stability. We have fixed points under different conditions:

(i) $p_0(0,0)$ is the fixed point;
(ii) $p_1(\frac{1}{2}(\sqrt{\alpha^2+4\alpha}-\alpha), \frac{1}{2}(\alpha^2+2\alpha-\alpha\sqrt{\alpha^2+4\alpha}))$;
(iii) $p_2(-\frac{1}{2}(\sqrt{\alpha^2+4\alpha}+\alpha), \frac{1}{2}(\alpha^2+2\alpha+\alpha\sqrt{\alpha^2+4\alpha}))$.

Model (4) is reformulated in the following manner:

$$\begin{cases} \varkappa_{n+1} = \eta(\varkappa_n, \gamma_n) = (1+\alpha h)\varkappa_n - h\varkappa_n\gamma_n - \alpha h\varkappa_n^2, \\ \gamma_{n+1} = \mu(\varkappa_n, \gamma_n) = (1-h)\gamma_n + h\varkappa_n^2. \end{cases} \tag{5}$$

At the point $p(\varkappa, \gamma)$, the Jacobian matrix (J) associated with model (5) is displayed as follows:

$$J(\varkappa, \gamma) = \begin{pmatrix} j_{11} & j_{12} \\ j_{21} & j_{22} \end{pmatrix}, \tag{6}$$

where

$$j_{11} = \frac{\partial\eta(\varkappa_n,\gamma_n)}{\partial\varkappa_n}|_{(\varkappa_n,\gamma_n)} = 1 + ((-2\varkappa+1)\alpha - \gamma)h, \; j_{12} = \frac{\partial\eta(\varkappa_n,\gamma_n)}{\partial\gamma_n}|_{(\varkappa_n,\gamma_n)} = -h\varkappa,$$

$$j_{21} = \frac{\partial\mu(\varkappa_n,\gamma_n)}{\partial\varkappa_n}|_{(\varkappa_n,\gamma_n)} = 2h\varkappa \text{ and } j_{22} = \frac{\partial\mu(\varkappa_n,\gamma_n)}{\partial\gamma_n}|_{(\varkappa_n,\gamma_n)} = 1 - h.$$

The equation that represents the characteristics is expressed in the following form:

$$\mathcal{R}^2 - T(\varkappa, \gamma)\mathcal{R} + D(\varkappa, \gamma) = 0. \tag{7}$$

The quadratic Equation (7) with a single variable, represented by

$$T(\varkappa, \gamma) = (j_{11} + j_{22}) \textit{ and } D(\varkappa, \gamma) = j_{11}j_{22} - j_{12}j_{21}.$$

Lemma 1 ([23])**.** *Let $\Gamma(\mathcal{R}) = \mathcal{R}^2 - T\mathcal{R} + D$. Assume that $\Gamma(1) > 0$, $\mathcal{R}_1$ and $\mathcal{R}_2$ are two roots of $\Gamma(\mathcal{R}) = 0$. Then*

(i) $|\mathcal{R}_1| < 1$, $|\mathcal{R}_2| < 1$ *if and only if* $\Gamma(-1) > 0$, $D < 1$.
(ii) $|\mathcal{R}_1| < 1$, $|\mathcal{R}_2| > 1$ *(or* $|\mathcal{R}_1| > 1$, $|\mathcal{R}_2| < 1$*) if and only if* $\Gamma(-1) < 0$.
(iii) $|\mathcal{R}_1| > 1$, $|\mathcal{R}_2| > 1$ *if and only if* $\Gamma(-1) > 0$, $D > 1$.
(iv) $\mathcal{R}_1 = -1$, $|\mathcal{R}_2| \neq 1$ *if and only if* $\Gamma(-1) = 0$, $T \neq 0, 2$.
(v) $\mathcal{R}_1, \mathcal{R}_2$ *are complex and* $|\mathcal{R}_1| = |\mathcal{R}_2| = 1$ *if and only if* $T^2 - 4D < 0$, $D = 1$.

Definition 1 ([23])**.** *The fixed point $p(x, y)$ is called*

(1) *Sink if* $|\mathcal{R}_1| < 1$ *and* $|\mathcal{R}_2| < 1$. *It is locally asymptotic stable.*
(2) *Saddle if* $|\mathcal{R}_1| < 1$ *and* $|\mathcal{R}_2| > 1$ *(or* $|\mathcal{R}_1| > 1$ *and* $|\mathcal{R}_2| < 1$*). It is locally unstable.*
(3) *Source if* $|\mathcal{R}_1| > 1$ *and* $|\mathcal{R}_2| > 1$. *It is locally unstable.*
(4) *Non-hyperbolic if either* $|\mathcal{R}_1| = 1$ *or* $|\mathcal{R}_2| = 1$.

By utilising Lemma 1 and Definition 1, we obtain the following results:

Theorem 1. *states the following properties for the simple fixed point* $p_0(0,0)$*:*
(1) *When* $0 < h < 2$, $p_0(0,0)$ *is a saddle point.*
(2) *When* $h = 2$, $p_0(0,0)$ *is non-hyperbolic fixed point.*
(3) *When* $h > 2$, $p_0(0,0)$ *is a source fixed point.*

Proof. The Jacobian matrix $J(p_0)$ at the point $p_0(0,0)$ is expressed in the following form:

$$J(p_0) = \begin{pmatrix} \alpha h + 1 & 0 \\ 0 & 1 - h \end{pmatrix}. \tag{8}$$

The matrix has two eigenvalues: $\mathcal{R}_1 = \alpha h + 1$ and $\mathcal{R}_2 = 1 - h$. It is clear that by applying Lemma 1, the result can be directly derived. □

Theorem 2. *(i) If any of the following sets of conditions is true, then* $p_1(\frac{1}{2}(\sqrt{\alpha^2 + 4\alpha} - \alpha), \frac{1}{2}(\alpha^2 + 2\alpha - \alpha\sqrt{\alpha^2 + 4\alpha}))$ *is asymptotically stable (sink):*
(i-1) $-2\sqrt{\psi} < \varphi < 0$ *and* $0 < h < -\frac{\varphi}{\psi}$, *where* $\varphi = \frac{\alpha^2}{2} - 1 - \frac{\alpha\sqrt{\alpha^2+4\alpha}}{2}$ *and* $\psi = \frac{\alpha^2}{2} + 2\alpha - \frac{\alpha\sqrt{\alpha^2+4\alpha}}{2}$.
(i-2) $\varphi < -2\sqrt{\psi}$ *and* $0 < h < \frac{-\varphi - \sqrt{\varphi^2 - 4\psi}}{\psi}$.
(ii) If any of the following sets of conditions is true, then $p_1(\frac{1}{2}(\sqrt{\alpha^2 + 4\alpha} - \alpha), \frac{1}{2}(\alpha^2 + 2\alpha - \alpha\sqrt{\alpha^2 + 4\alpha}))$ *is unstable (source):*
(ii-1) $-2\sqrt{\psi} < \varphi$ *and* $h > -\frac{\varphi}{\psi}$.
(ii-2) $\varphi < -2\sqrt{\psi}$ *and* $h > \frac{-\varphi + \sqrt{\varphi^2 - 4\psi}}{\psi}$.
(iii) If any of the following sets of conditions is true, then $p_1(\frac{1}{2}(\sqrt{\alpha^2 + 4\alpha} - \alpha), \frac{1}{2}(\alpha^2 + 2\alpha - \alpha\sqrt{\alpha^2 + 4\alpha}))$ *is unstable (non-hyperbolic):*
(iii-1) $\varphi < -2\sqrt{\psi}$ *and* $h = \frac{-\varphi \pm \sqrt{\varphi^2 - 4\psi}}{\psi}$ *and* $h \neq -\frac{2}{\varphi}, -\frac{4}{\varphi}$.
(iii-2) $-2\sqrt{\psi} < \varphi$ *and* $h = -\frac{\varphi}{\psi}$.
(iv) The fixed point $p_1(\frac{1}{2}(\sqrt{\alpha^2 + 4\alpha} - \alpha), \frac{1}{2}(\alpha^2 + 2\alpha - \alpha\sqrt{\alpha^2 + 4\alpha}))$ *is unstable (saddle point) if*
(iv-1) $\phi < -2\sqrt{\psi}$.
(iv-2) $\frac{-\varphi - \sqrt{\varphi^2 - 4\psi}}{\psi} < h < \frac{-\varphi + \sqrt{\phi^2 - 4\psi}}{\psi}$.

Proof. The Jacobian matrix at $p_1(\frac{1}{2}(\sqrt{\alpha^2 + 4\alpha} - \alpha), \frac{1}{2}(\alpha^2 + 2\alpha - \alpha\sqrt{\alpha^2 + 4\alpha}))$ has the form

$$J(\hat{\varkappa}, \hat{\gamma}) = \begin{bmatrix} j_{11} & j_{12} \\ j_{21} & j_{22} \end{bmatrix},$$

where

$$j_{11} = 1 + \frac{\alpha h(\alpha - \sqrt{\alpha^2 + 4\alpha})}{2}, \quad j_{12} = -\frac{h(\sqrt{\alpha^2 + 4\alpha} - \alpha)}{2},$$
$$j_{21} = h(\sqrt{\alpha^2 + 4\alpha} - \alpha) \text{ and } j_{22} = 1 - h.$$

Let

$$\mathcal{R}^2 - (2 + \phi h)\mathcal{R} + (1 + \phi h + \psi h^2) = 0,$$

where

$$\phi = \frac{\alpha^2}{2} - 1 - \frac{\alpha\sqrt{\alpha^2+4\alpha}}{2},$$

and

$$\psi = \frac{\alpha^2}{2} + 2\alpha - \frac{\alpha\sqrt{\alpha^2+4\alpha}}{2},$$

since

$$\Gamma(\mathcal{R}) = \mathcal{R}^2 - T\mathcal{R} + D,$$

where

$$T = j_{11} + j_{22} \text{ and } D = -j_{12}j_{21} + j_{11}j_{22},$$

then, we obtain

$$\Gamma(-1) = 4 + 2\phi h + \psi h^2. \tag{9}$$

According to Lemma 1, the fixed point is locally asymptotically stable if and only if $D < 1$ and $\Gamma(-1) > 0$. Furthermore, the fixed point is non-hyperbolic if and only if $T \neq 0$ or 2 and $\Gamma(-1) = 0$. Theorem 2 is obtained by calculating (9), thus completing the proof. □

According to Theorem 2, it is evident that if condition (iii-1) holds, one of the eigenvalues of the fixed point $p_1(\frac{1}{2}(\sqrt{\alpha^2+4\alpha}-\alpha), \frac{1}{2}(\alpha^2+2\alpha-\alpha\sqrt{\alpha^2+4\alpha}))$ is -1, while the other eigenvalue is neither 1 nor -1. When condition (iii-2) of Theorem 2 is true, the eigenvalues of the fixed point $p_1(\frac{1}{2}(\sqrt{\alpha^2+4\alpha}-\alpha), \frac{1}{2}(\alpha^2+2\alpha-\alpha\sqrt{\alpha^2+4\alpha}))$ are a pair of complex conjugate numbers with equal modulus.
Let

$$F_{1P_1} = \left\{ (\alpha, h) : h = h_1 = \frac{-\phi-\sqrt{\phi^2-4\psi}}{\psi}, \phi < -2\sqrt{\psi}, \alpha, h > 0 \right\},$$

and

$$F_{2P_1} = \left\{ (\alpha, h) : h = h_1' = \frac{-\phi+\sqrt{\phi^2-4\psi}}{\psi}, \phi < -2\sqrt{\psi}, \alpha, h > 0 \right\}.$$

In a small neighborhood of F_{1P_1} or F_{2P_1}, the positive fixed point $p_1(\frac{1}{2}(\sqrt{\alpha^2+4\alpha}-\alpha), \frac{1}{2}(\alpha^2+2\alpha-\alpha\sqrt{\alpha^2+4\alpha}))$ may undergo period-doubling bifurcation when the parameters are varied.

$$N_{P_1} = \left\{ (\alpha, h) : h = h_2 = -\frac{\phi}{\psi}, -2\sqrt{\psi} < \phi < 0, \alpha, h > 0 \right\}.$$

In a small neighborhood of N_{P_1}, the positive fixed point $p_1(\frac{1}{2}(\sqrt{\alpha^2+4\alpha}-\alpha), \frac{1}{2}(\alpha^2+2\alpha-\alpha\sqrt{\alpha^2+4\alpha}))$ may undergo Neimark–Sacker bifurcation when the parameters are varied.

3. Bifurcations Analysis

In this section, the discussion on fixed points is divided into two parts. First, we examine the pitchfork bifurcation when the trivial fixed point is $p_0(0,0)$. Then, we analyze the case of the positive fixed point $p_1(\frac{1}{2}(\sqrt{\alpha^2+4\alpha}-\alpha), \frac{1}{2}(\alpha^2+2\alpha-\alpha\sqrt{\alpha^2+4\alpha}))$, we discuss the PB and NB separately. Then, by applying the center manifold theorem and bifurcation theory [24], we establish the conditions for the existence of these various bifurcations.

3.1. Pitchfork Bifurcation

If $\alpha = 0$, then the Jacobian matrix $J(P_0)$ has two eigenvalues: $\mathcal{R}_1 = 1$ and $\mathcal{R}_2 = 1 - h$. When $h \neq 2$, then $|\mathcal{R}_2| \neq 1$, indicating the conditions for the appearance of a pitchfork bifurcation at P_0. These conditions are represented by the following theorem:

Theorem 3. *If $\alpha = 0$, $h \neq 2$, then the model (4) is subject to a pitchfork bifurcation at $P_0(0,0)$ and has only one fixed point.*

Proof. Let us consider the parameter $\sigma_n = \alpha$ as a newly introduced dependent variable. Then, the model (4) becomes

$$\begin{pmatrix} \varkappa_{n+1} \\ \gamma_{n+1} \\ \sigma_{n+1} \end{pmatrix} \to \begin{pmatrix} 1 & 0 & 0 \\ 0 & 1-h & 0 \\ 0 & 0 & 1 \end{pmatrix} \begin{pmatrix} \varkappa_n \\ \gamma_n \\ \sigma_n \end{pmatrix} + \begin{pmatrix} \hat{f}(\varkappa_n, \gamma_n, \sigma_n) \\ \hat{g}(\varkappa_n, \gamma_n, \sigma_n) \\ 0 \end{pmatrix}, \tag{10}$$

where

$$\begin{aligned} \hat{f}(\varkappa_n, \gamma_n, \sigma_n) &= -h\varkappa_n\gamma_n + h\varkappa_n\sigma_n - h\varkappa_n^2\sigma_n, \\ \hat{g}(\varkappa_n, \gamma_n, \sigma_n) &= h\varkappa_n^2. \end{aligned} \tag{11}$$

Let

$$\gamma_n = s(\varkappa_n, \sigma_n) = \tilde{\delta}_1\varkappa_n^2 + \tilde{\delta}_2\varkappa_n\sigma_n + \tilde{\delta}_3\sigma_n^2 + o((|\varkappa_n| + |\sigma_n|)^3). \tag{12}$$

The center manifold must satisfy

$$W(s(\varkappa_n, \sigma_n)) = s(\varkappa_n + f(\varkappa_n, (\varkappa_n, \sigma_n), \sigma_n), \sigma_{n+1}) - (1-h)s(\varkappa_n, \sigma_n) - g(\varkappa_n, (\varkappa_n, \sigma_n), \sigma_{n+1}) = 0. \tag{13}$$

Thus, we can obtain that

$$\tilde{\delta}_1 = 1, \tilde{\delta}_2 = 0 \; and \; \tilde{\delta}_3 = 0. \tag{14}$$

And the map is limited to the central manifold that was given by

$$\hat{f}_1 = \varkappa_n - h\varkappa_n^3 + h\varkappa_n\sigma_n - h\varkappa_n^2\sigma_n + o((|\varkappa_n| + |\sigma_n|)^3). \tag{15}$$

Since

$$\frac{\partial^2 \hat{f}_1}{\partial \varkappa_n \partial \sigma_n} = h \neq 0 \;\; and \;\; \frac{\partial^3 \hat{f}_1}{\partial \varkappa_n^3} = -6h \neq 0.$$

A pitchfork bifurcation occurs at the point $P_0(0,0)$ in model (4). This concludes the proof. □

3.2. Period-Doubling Bifurcation

This study examines the PB of the discrete–time model (4) with respect to the fixed point $p_1(\frac{1}{2}(\sqrt{\alpha^2+4\alpha} - \alpha), \frac{1}{2}(\alpha^2 + 2\alpha - \alpha\sqrt{\alpha^2+4\alpha}))$. When the parameters are varied in a small neighborhood of F_{1P_1}, similar arguments can be applied. The same applies to the case of F_{2P_1}. We consider model (4) with $(\alpha, h) \in F_{1P_1}$ by selecting the parameters (α, h) arbitrarily from the set F_{1P_1} described by

$$\begin{cases} \varkappa_{n+1} = \varkappa_n + h_1(\alpha\varkappa_n(1-\varkappa_n) - \varkappa_n\gamma_n), \\ \gamma_{n+1} = \gamma_n - h_1({\varkappa_n}^2 - \gamma_n). \end{cases} \tag{16}$$

Then model (16) has a fixed point $p_1(\frac{1}{2}(\sqrt{\alpha^2+4\alpha} - \alpha), \frac{1}{2}(\alpha^2 + 2\alpha - \alpha\sqrt{\alpha^2+4\alpha}))$ with eigenvalues $\mathcal{R}_1 = -1$ and $\mathcal{R}_2 = 3 + \phi h_1$ with $|\mathcal{R}_2| \neq 1$ by Theorem 2.

$$\begin{cases} \varkappa_{n+1} = \varkappa_n + (h_1 + h_*)(\alpha\varkappa_n(1-\varkappa_n) - \varkappa_n\gamma_n), \\ \gamma_{n+1} = \gamma_n - (h_1 + h_*)({\varkappa_n}^2 - \gamma_n). \end{cases} \tag{17}$$

Here, $|h_*| << 1$ represents a small disturbance parameter.

Suppose that $u = \varkappa - \hat{\varkappa}$, $v = \gamma - \hat{\gamma}$. Subsequently, we perform a transformation to relocate the fixed point $p_1(\frac{1}{2}(\sqrt{\alpha^2+4\alpha} - \alpha), \frac{1}{2}(\alpha^2 + 2\alpha - \alpha\sqrt{\alpha^2+4\alpha}))$ or $p_1(\hat{\varkappa}, \hat{\gamma})$ of the model (17) to the origin.

Consequently, we obtain

$$\begin{pmatrix} u \\ v \end{pmatrix} \to \begin{pmatrix} \mathcal{E}_{11}u + \mathcal{E}_{12}v + \mathcal{E}_{13}uv + \mathcal{E}_{14}u^2 \\ +\mathcal{P}_1uh + \mathcal{P}_2vh + \mathcal{P}_3uvh + \mathcal{P}_4u^2h \\ \mathcal{E}_{21}u + \mathcal{E}_{22}v + \mathcal{E}_{23}u^2 \\ +\mathcal{P}_5uh + \mathcal{P}_6vh + \mathcal{P}_7u^2h \end{pmatrix}, \tag{18}$$

where

$$
\begin{array}{lll}
\mathcal{E}_{11}=1+((1-2\hat{\varkappa})\alpha-\hat{\gamma})h, & \mathcal{E}_{12}=-h\hat{\varkappa}, & \mathcal{E}_{13}=-h \\
\mathcal{E}_{14}=-\alpha h, & \mathcal{P}_{1}=(1-2\hat{\varkappa})\alpha-\hat{\gamma}, & \mathcal{P}_{2}=-\hat{\varkappa} \\
\mathcal{P}_{3}=-1, & \mathcal{P}_{4}=-\alpha, & \\
\mathcal{E}_{21}=2h\hat{\varkappa}, & \mathcal{E}_{22}=1-h, & \mathcal{E}_{23}=h, \\
\mathcal{P}_{5}=2\hat{\varkappa}, & \mathcal{P}_{6}=-1 \quad and \quad \mathcal{P}_{7}=1, &
\end{array}
\tag{19}
$$

and $h=h_1$.

We construct an invertible matrix

$$
\mathcal{M}=\begin{pmatrix} \mathcal{E}_{12} & \mathcal{E}_{12} \\ -1-\mathcal{E}_{11} & \mathcal{R}_2-\mathcal{E}_{11} \end{pmatrix},
$$

and we apply the translation $(\varkappa,\gamma)^T=\mathcal{M}(\bar{\varkappa},\bar{\gamma})^T$. As a result, map (18) can be transformed into

$$
\begin{pmatrix} \varkappa \\ \gamma \end{pmatrix} \rightarrow \begin{pmatrix} -1 & 0 \\ 0 & \mathcal{R}_2 \end{pmatrix}\begin{pmatrix} \bar{\varkappa} \\ \bar{\gamma} \end{pmatrix}+\begin{pmatrix} f(u,v,h_*) \\ g(u,v,h_*) \end{pmatrix},
\tag{20}
$$

where

$$
\begin{aligned}
f(u,v,h_*) \;=\; & \frac{(\mathcal{E}_{14}(\mathcal{R}_2-\mathcal{E}_{11})-\mathcal{E}_{12}\mathcal{E}_{23})}{\mathcal{E}_{12}(1+\mathcal{R}_2)}u^2+\frac{(\mathcal{R}_2-\mathcal{E}_{11})\mathcal{E}_{13}}{\mathcal{E}_{12}(1+\mathcal{R}_2)}uv \\
& +\frac{(\mathcal{P}_4(\mathcal{R}_2-\mathcal{E}_{11})-\mathcal{P}_7\mathcal{E}_{12})}{\mathcal{E}_{12}(1+\mathcal{R}_2)}hu^2+\frac{\mathcal{P}_3(\mathcal{R}_2-\mathcal{E}_{11})}{\mathcal{E}_{12}(1+\mathcal{R}_2)}huv \\
& +\frac{(\mathcal{P}_1(\mathcal{R}_2-\mathcal{E}_{11})-\mathcal{P}_5\mathcal{E}_{12})}{\mathcal{E}_{12}(1+\mathcal{R}_2)}hu+\frac{(\mathcal{P}_2(\mathcal{R}_2-\mathcal{E}_{11})-\mathcal{P}_6\mathcal{E}_{12})}{\mathcal{E}_{12}(1+\mathcal{R}_2)}hv \\
& +o((|u|+|v|+|h_1|)^4),
\end{aligned}
\tag{21}
$$

and

$$
\begin{aligned}
g(u,v,h_*) \;=\; & \frac{(\mathcal{E}_{14}(1+\mathcal{E}_{11})+\mathcal{E}_{12}\mathcal{E}_{23})}{\mathcal{E}_{12}(1+\mathcal{R}_2)}u^2+\frac{\mathcal{E}_{13}(1+\mathcal{E}_{11})}{\mathcal{E}_{12}(1+\mathcal{R}_2)}uv \\
& +\frac{(\mathcal{P}_4(1+\mathcal{E}_{11})+\mathcal{E}_{12}\mathcal{P}_7)}{\mathcal{E}_{12}(1+\mathcal{R}_2)}hu^2+\frac{\mathcal{P}_3(1+\mathcal{E}_{11})}{\mathcal{E}_{12}(1+\mathcal{R}_2)}huv \\
& +\frac{(\mathcal{P}_1(1+\mathcal{E}_{11})+\mathcal{E}_{12}\mathcal{P}_5)}{\mathcal{E}_{12}(1+\mathcal{R}_2)}hu+\frac{(\mathcal{P}_2(1+\mathcal{E}_{11})+\mathcal{E}_{12}\mathcal{P}_6)}{\mathcal{E}_{12}(1+\mathcal{R}_2)}hv \\
& +o((|u|+|v|+|h_1|)^4).
\end{aligned}
$$

With $u=\mathcal{E}_{12}\bar{\varkappa}+\mathcal{E}_{12}\bar{\gamma}$ and $v=-(1+\mathcal{E}_{11})\bar{\varkappa}+(\mathcal{R}_2-\mathcal{E}_{11})\bar{\gamma}$. The dynamics of the fixed point $(\bar{\varkappa},\bar{\gamma})=(0,0)$ at $h_*=0$ are then computed using the center manifold theorem, as presented in [25]. Consequently, a center manifold $W^c(0,0)$ of map (20) arises. It can be described as follows:

$$
W^c(0,0)=(\bar{\varkappa},\bar{\gamma})|\bar{\gamma}=s(\bar{\varkappa},h_*),s(0,0)=0,Dh(0,0)=0.
$$

Assume that

$$
s(\bar{\varkappa},h_*)=c_1\bar{\varkappa}^2+c_2\bar{\varkappa}h_*+c_3h_*^2+o((|u|+|h_*|)^3),
\tag{22}
$$

where $o((|u|+|h_*|)^3)$ is a function with variables of at least three orders $(\bar{\varkappa}, h_*)$ and

$$c_1 = \frac{\mathcal{E}_{12}^2\mathcal{E}_{23} + \mathcal{E}_{14}\mathcal{E}_{12} + (\mathcal{E}_{14}\mathcal{E}_{12} - 2\mathcal{E}_{13})\mathcal{E}_{11} - (\mathcal{E}_{11}^2 + 1)\mathcal{E}_{13}}{(1-\mathcal{R}_2^2)},$$

$$\begin{aligned} c_2 &= \frac{\mathcal{P}_2(1+\mathcal{E}_{11})^2 - \mathcal{E}_{12}^2\mathcal{P}_5 - (1+\mathcal{E}_{11})(\mathcal{P}_1 - \mathcal{P}_6)\mathcal{E}_{12}}{\mathcal{E}_{12}(1+\mathcal{R}_2)^2}, \\ c_3 &= 0. \end{aligned}$$

Therefore, the map (20), when restricted to $W^c(0,0)$, can be expressed as follows:

$$F : \bar{\varkappa} \to -\bar{\varkappa} + s_1\bar{\varkappa}^2 + s_2\bar{\varkappa}h_* + s_3\bar{\varkappa}^2 h_* + s_4\bar{\varkappa}h_*^2 + s_5\bar{\varkappa}^3 + O((|\bar{\varkappa}| + |h_*|^4),$$

where

$$s_1 = \tfrac{1}{\mathcal{R}_2+1}((\mathcal{R}_2 - \mathcal{E}_{11})(\mathcal{E}_{12}\mathcal{E}_{14} - (1+\mathcal{E}_{11})\mathcal{E}_{13}) - \mathcal{E}_{12}^2\mathcal{E}_{23},$$

$$s_2 = \tfrac{1}{\mathcal{E}_{12}(\mathcal{R}_2+1)}((\mathcal{R}_2 - \mathcal{E}_{11})(\mathcal{E}_{12}\mathcal{P}_1 - (1+\mathcal{E}_{11})\mathcal{P}_2) - (\mathcal{E}_{12}\mathcal{P}_5 - (1+\mathcal{E}_{11})\mathcal{P}_6)\mathcal{E}_{12},$$

$$\begin{aligned} s_3 = \tfrac{1}{\mathcal{E}_{12}(\mathcal{R}_2+1)}&(((2\mathcal{E}_{14}c_2 + \mathcal{P}_4)\mathcal{R}_2 - (\mathcal{P}_4 + 2\mathcal{E}_{14}c_2)\mathcal{E}_{11} - c_1\mathcal{P}_5)\mathcal{E}_{12}^2 \\ &- (\mathcal{E}_{12}^3(2\mathcal{E}_{23}c_2 + \mathcal{P}_7) + (\mathcal{E}_{11} - \mathcal{R}_2)((2\mathcal{E}_{13}c_2 + \mathcal{P}_3)\mathcal{E}_{11} - \mathcal{E}_{13}c_2\mathcal{R}_2 \\ &+ (\mathcal{P}_6 - \mathcal{P}_1)c_1 + \mathcal{E}_{13}c_2 + \mathcal{P}_3)\mathcal{E}_{12} + c_1\mathcal{P}_2(\mathcal{R}_2 - \mathcal{E}_{11})^2), \end{aligned}$$

$$s_4 = \tfrac{1}{\mathcal{E}_{12}(\mathcal{R}_2+1)}((-\mathcal{E}_{12}^2\mathcal{P}_5 + (\mathcal{P}_1 - \mathcal{P}_6)(\mathcal{R}_2 - \mathcal{E}_{11})\mathcal{E}_{12} + \mathcal{P}_2(\mathcal{R}_2 - \mathcal{E}_{11})^2)c_2),$$

and

$$s_5 = \tfrac{1}{(\mathcal{R}_2+1)}(c_1(\mathcal{E}_{13}(\mathcal{R}_2 - \mathcal{E}_{11})(\mathcal{R}_2 - 2\mathcal{E}_{11} - 1) - 2\mathcal{E}_{12}(\mathcal{E}_{11}\mathcal{E}_{14} + \mathcal{E}_{12}\mathcal{E}_{23} - \mathcal{E}_{14}\mathcal{R}_2))).$$

Let

$$\Psi_1 = \left(\frac{\partial^2 F}{\partial\bar{\varkappa}\partial h_*} + \frac{1}{2}\frac{\partial F}{\partial h_*}\frac{\partial^2 F}{\partial\bar{\varkappa}^2}\right)|_{(0,0)} = s_2,$$

and

$$\Psi_2 = \left(\frac{1}{6}\frac{\partial^3 F}{\partial\bar{\varkappa}^3} + (\frac{1}{2}\frac{\partial^2 F}{\partial\bar{\varkappa}^2})^2\right)|_{(0,0)} = s_1^2 + s_5.$$

Based on the previous argument, we have the following theorem:

Theorem 4. *If* $\Psi_1 \neq 0$ *and* $\Psi_2 \neq 0$, *then model (4) is subject to a PB at the unique positive fixed point* $p_1(\frac{1}{2}(\sqrt{\alpha^2+4\alpha} - \alpha), \frac{1}{2}(\alpha^2 + 2\alpha - \alpha\sqrt{\alpha^2+4\alpha}))$ *when the parameter h differs in a small neighborhood of* F_{P_1}. *Furthermore, if* $\Psi_2 > 0$ *(respectively,* $\Psi_2 < 0$*), then the period-2 orbits that biforkeds from* $p_1(\frac{1}{2}(\sqrt{\alpha^2+4\alpha} - \alpha), \frac{1}{2}(\alpha^2 + 2\alpha - \alpha\sqrt{\alpha^2+4\alpha}))$ *are stable (respectively, unstable).*

3.3. Neimark–Sacker Bifurcation

We now delve into the NB of $p_1(\frac{1}{2}(\sqrt{\alpha^2+4\alpha} - \alpha), \frac{1}{2}(\alpha^2 + 2\alpha - \alpha\sqrt{\alpha^2+4\alpha}))$ when the parameters (α, h) vary within a small neighborhood of N_{p_1}. We examine model (4) with $(\alpha, h) \in N_{p_1}$, defined by the following expression:

$$\begin{cases} \varkappa_{n+1} = \varkappa_n + h_2(\alpha\varkappa_n(1-\varkappa_n) - \varkappa_n\gamma_n), \\ \gamma_{n+1} = \gamma_n - h_2(\varkappa_n{}^2 - \gamma_n). \end{cases} \tag{23}$$

Model (23) has a fixed point $p_1(\frac{1}{2}(\sqrt{\alpha^2+4\alpha} - \alpha), \frac{1}{2}(\alpha^2 + 2\alpha - \alpha\sqrt{\alpha^2+4\alpha}))$. Then, by choosing $\bar{h}_*$ as a bifurcation parameter, we consider a perturbation of (23) as follows:

$$\begin{cases} \varkappa_{n+1} = \varkappa_n + (h_2 + \bar{h}_*)(\alpha\varkappa_n(1-\varkappa_n) - \varkappa_n\gamma_n), \\ \gamma_{n+1} = \gamma_n - (h_2 + \bar{h}_*)({\varkappa_n}^2 - \gamma_n). \end{cases} \tag{24}$$

Here, $|\bar{h}_*| << 1$ represents a small disturbance parameter.

Suppose that $\upsilon = \varkappa - \hat{\varkappa}$, $\nu = \gamma - \hat{\gamma}$. Then, we transform the positive fixed point $p_1(\frac{1}{2}(\sqrt{\alpha^2+4\alpha}-\alpha), \frac{1}{2}(\alpha^2+2\alpha-\alpha\sqrt{\alpha^2+4\alpha}))$ of the model (24) into the origin. Then, we have

$$\begin{pmatrix} \upsilon \\ \nu \end{pmatrix} \rightarrow \begin{pmatrix} \mathcal{E}_{11}\upsilon + \mathcal{E}_{12}\upsilon + \mathcal{E}_{13}\upsilon\nu + \mathcal{E}_{14}\upsilon^2 \\ \mathcal{E}_{21}\upsilon + \mathcal{E}_{22}\nu + \mathcal{E}_{23}\upsilon^2 \end{pmatrix}. \tag{25}$$

Here, $\mathcal{E}_{11}$, $\mathcal{E}_{12}$, $\mathcal{E}_{13}$, $\mathcal{E}_{14}$, $\mathcal{E}_{21}$, $\mathcal{E}_{22}$, $\mathcal{E}_{23}$ are obtained in (19) by substituting h with $h_2 + \bar{h}_*$. Then, model (24) has a fixed point $p_1(\hat{\varkappa}, \hat{\gamma})$, where $\hat{\varkappa} = \frac{1}{2}(\sqrt{\alpha^2+4\alpha}-\alpha)$, $\hat{\gamma} = \frac{1}{2}(\alpha^2+2\alpha-\alpha\sqrt{\alpha^2+4\alpha})$.

The characteristic equation for $p_1(\hat{\varkappa}, \hat{\gamma})$ is given by the model (24):

$$\mathcal{R}^2 - p(\bar{h}_*)\mathcal{R} + q(\bar{h}_*) = 0,$$

where

$$p(\bar{h}_*) = 2 + (\alpha - 2\hat{\varkappa}\alpha - \hat{\gamma} - 1)(h_2 + \bar{h}_*),$$

and

$$q(\bar{h}_*) = 1 + ((2\hat{\varkappa}-1)\alpha + 2\hat{\varkappa}^2 + \hat{\gamma})(h_2 + \bar{h}_*)^2 + (\alpha - 2\hat{\varkappa}^2\alpha - \hat{\gamma} - 1)(h_2 + \bar{h}_*).$$

Since parameters $(\alpha, h) \in N_{p_1}$, the eigenvalues of $p_1(\hat{\varkappa}, \hat{\gamma})$ are a pair of complex conjugate numbers $\mathcal{R}, \overline{\mathcal{R}}$ with model (4) by Theorem 2, where

$$\begin{aligned} \mathcal{R}, \overline{\mathcal{R}} &= -\frac{p(\bar{h}_*)}{2} \pm i\frac{\sqrt{4q(\bar{h}_*) - p^2(\bar{h}_*)}}{2}, \\ &= 1 + \frac{\phi(h_2 + \bar{h}_*)}{2} \pm \frac{i(h_2 + \bar{h}_*)\sqrt{4\psi - \phi^2}}{2}. \end{aligned}$$

Then we obtain

$$|\mathcal{R}| = \sqrt{q(\bar{h}_*)}, \ell = \frac{d|\mathcal{R}|}{d\bar{h}_*}|_{\bar{h}_*=0} = \frac{-\phi}{2} > 0.$$

Additionally, $\bar{h}_* = 0$, $\mathcal{R}^n$ and $\overline{\mathcal{R}}^n \neq 1$, $n = 1, 2, 3, 4$, which is equivalent to $p(0) \neq -2, 0, 1$ and 2. Note, that $(\alpha, h) \in N_{p_1}$, so $p(0) \neq -2$ and 2. As a result, we only require satisfactory $p(0) \neq 0$ and 1, which leads to

$$\phi^2 \neq 2\psi, 3\psi. \tag{26}$$

Afterward, we proceed to discuss map (25) when $\bar{h}_* = 0$. Put

$$m = 1 + \frac{\phi h}{2},$$

and

$$\omega = \frac{h\sqrt{4\psi - \phi^2}}{2}.$$

Using the translation

$$\begin{pmatrix} \upsilon \\ \nu \end{pmatrix} = \begin{pmatrix} \mathcal{E}_{12} & 0 \\ m - \mathcal{E}_{11} & -\omega \end{pmatrix} \begin{pmatrix} \check{\upsilon} \\ \check{\nu} \end{pmatrix},$$

the map (25) becomes

$$\begin{pmatrix} \check{v} \\ \check{\nu} \end{pmatrix} \to \begin{pmatrix} m & -\omega \\ \omega & m \end{pmatrix} \begin{pmatrix} \check{v} \\ \check{\nu} \end{pmatrix} + \begin{pmatrix} \check{\mathfrak{f}}(\check{v}, \check{\nu}, h_*) \\ \check{\vartheta}(\check{v}, \check{\nu}, h_*) \end{pmatrix}, \tag{27}$$

where

$$\check{\mathfrak{f}}(\check{v}, \check{\nu}, h_*) = \frac{1}{\mathcal{E}_{12}}(\mathcal{E}_{13} v\nu + \mathcal{E}_{14} v^2),$$

and

$$\check{\vartheta}(\check{v}, \check{\nu}, h_*) = \frac{((m - \mathcal{E}_{11})\mathcal{E}_{14} - \mathcal{E}_{12}\mathcal{E}_{23})v^2}{\mathcal{E}_{12}\omega} + \frac{(m - \mathcal{E}_{11})\mathcal{E}_{13} v\nu}{\mathcal{E}_{12}\omega}.$$

We have found the following:

$$\check{\mathfrak{f}}_{\check{v}\check{v}} = 2((m - \mathcal{E}_{11})\mathcal{E}_{13} + \mathcal{E}_{12}\mathcal{E}_{14}), \quad \check{\mathfrak{f}}_{\check{v}\check{\nu}} = -\omega\mathcal{E}_{13}, \quad \check{\mathfrak{f}}_{\check{\nu}\check{\nu}} = 0,$$

$$\check{\mathfrak{f}}_{\check{v}\check{v}\check{v}} = 0, \quad \check{\mathfrak{f}}_{\check{v}\check{v}\check{\nu}} = 0, \quad \check{\mathfrak{f}}_{\check{v}\check{\nu}\check{\nu}} = 0, \quad \check{\mathfrak{f}}_{\check{\nu}\check{\nu}\check{\nu}} = 0,$$

and

$$\check{\vartheta}_{\check{v}\check{v}} = \frac{2}{\omega}(\mathcal{E}_{12}\mathcal{E}_{14}(m - \mathcal{E}_{11}) + (m - \mathcal{E}_{11})^2\mathcal{E}_{13} - \mathcal{E}_{12}^2\mathcal{E}_{23}),$$

$$\check{\vartheta}_{\check{v}\check{\nu}} = -(m - \mathcal{E}_{11})\mathcal{E}_{13},$$

$$\check{\vartheta}_{\check{\nu}\check{\nu}} = 0, \quad \check{\vartheta}_{\check{v}\check{v}\check{v}} = 0, \quad \check{\vartheta}_{\check{v}\check{v}\check{\nu}} = 0, \quad \check{\vartheta}_{\check{v}\check{\nu}\check{\nu}} = 0, \quad \check{\vartheta}_{\check{\nu}\check{\nu}\check{\nu}} = 0.$$

If the discriminant quantity is non-zero, map (27) may undergo the NB.

$$\xi = Re[\frac{(1 - 2\mathcal{R})\bar{\mathcal{R}}^2}{1 - \mathcal{R}}\Phi_{11}\Phi_{20}] + \frac{1}{2}|\Phi_{11}|^2 + |\Phi_{02}|^2 - Re(\bar{\mathcal{R}}\Phi_{21}),$$

where

$$\begin{aligned}
\Phi_{20} &= \frac{1}{8}[\check{\mathfrak{f}}_{\check{v}\check{v}} - \check{\mathfrak{f}}_{\check{\nu}\check{\nu}} + 2\check{\vartheta}_{\check{v}\check{\nu}} + i(\check{\vartheta}_{\check{v}\check{v}} - \check{\vartheta}_{\check{\nu}\check{\nu}} - 2\check{\mathfrak{f}}_{\check{v}\check{\nu}})], \\
\Phi_{11} &= \frac{1}{4}[\check{\mathfrak{f}}_{\check{v}\check{v}} + \check{\mathfrak{f}}_{\check{\nu}\check{\nu}} + i(\check{\vartheta}_{\check{v}\check{v}} + \check{\vartheta}_{\check{\nu}\check{\nu}})], \\
\Phi_{02} &= \frac{1}{8}[\check{\mathfrak{f}}_{\check{v}\check{v}} - \check{\mathfrak{f}}_{\check{\nu}\check{\nu}} - 2\check{\vartheta}_{\check{v}\check{\nu}} + i(\check{\vartheta}_{\check{v}\check{v}} - \check{\vartheta}_{\check{\nu}\check{\nu}} + 2\check{\mathfrak{f}}_{\check{v}\check{\nu}})], \\
\Phi_{21} &= \frac{1}{16}[\check{\mathfrak{f}}_{\check{v}\check{v}\check{v}} + \check{\mathfrak{f}}_{\check{v}\check{\nu}\check{\nu}} + \check{\vartheta}_{\check{v}\check{v}\check{\nu}} + \check{\vartheta}_{\check{\nu}\check{\nu}\check{\nu}} + i(\check{\vartheta}_{\check{v}\check{v}\check{v}} + \check{\vartheta}_{\check{v}\check{\nu}\check{\nu}} - \check{\mathfrak{f}}_{\check{v}\check{v}\check{\nu}} - \check{\mathfrak{f}}_{\check{\nu}\check{\nu}\check{\nu}})].
\end{aligned}$$

Considering this study and the NB theorem described in [24,26], we can now present the following theorem:

Theorem 5. *If condition (26) is satisfied and $\xi \neq 0$, Model (4) undergoes an NB at the fixed point $p_1(\frac{1}{2}(\sqrt{\alpha^2 + 4\alpha} - \alpha), \frac{1}{2}(\alpha^2 + 2\alpha - \alpha\sqrt{\alpha^2 + 4\alpha}))$ when the parameter h varies within a small neighborhood of N_{p_1}. Additionally, if $\xi < 0$ (respectively, $\xi > 0$), an attracting (respectively, repelling) invariant closed curve bifurcates from the fixed point for $h > h_2$ (respectively, $h < h_2$).*

4. Control of Chaos

In this section, the utilization of different bifurcation parameters significantly enhances our ability to comprehensively analyze the system's behavior. By selecting independent parameters, we can isolate their influences and gain insights into their effects on the system's dynamics. This approach enables us to examine the system's sensitivity to various parameters, identify those with a significant impact on bifurcations, and develop a deeper understanding of its behavior under diverse conditions. Choosing multiple parameters makes the study practical and feasible, as some may be controlled or measured in experiments. Additionally, effective ecological conservation management solutions can be devised to preserve these intricate ecosystems. Chaotic dynamics within a system can lead to instabilities and undesirable behaviors. Therefore, effective techniques for chaos control are crucial for mitigating harmful chaotic behaviors. Regulating chaotic dynamics towards a periodic orbit or a fixed point is necessary to improve system performance. We applied the feedback control method known as OGY, as documented in the literature [27,28], to model (4). The basic aim is to make small, time-dependent linear perturbations to the control parameter α in order to nudge the state towards the stable manifold of the desired fixed point, thus controlling the chaos resulting from the NB and PB at the fixed point of model (4). We utilize the OGY technique to express model (4) as follows:

$$\begin{aligned} \varkappa_{n+1} &= (1+\alpha h)\varkappa_n - \varkappa_n \gamma_n - \alpha h \varkappa_n^2 = f(\varkappa_n, \gamma_n, \alpha), \\ \gamma_{n+1} &= (1-\varkappa_n)\gamma_n + \alpha \varkappa_n^2 = g(\varkappa_n, \gamma_n, \alpha). \end{aligned} \tag{28}$$

Here, α is treated as the chaos control parameter. Furthermore, we assume that α lies within the range $\alpha \in (\alpha_0 - \delta, \alpha_0 + \delta)$, where $\delta > 0$ and α_0 represents the nominal value of α. Moreover, we consider $p_1(\hat{\varkappa}, \hat{\gamma}) = p_1(\frac{1}{2}(\sqrt{\alpha^2+4\alpha} - \alpha), \frac{1}{2}(\alpha^2 + 2\alpha - \alpha\sqrt{\alpha^2+4\alpha}))$ as the fixed point of model (4). In the neighbourhood of the fixed point $p_1(\hat{\varkappa}, \hat{\gamma}) = p_1(\frac{1}{2}(\sqrt{\alpha^2+4\alpha} - \alpha), \frac{1}{2}(\alpha^2 + 2\alpha - \alpha\sqrt{\alpha^2+4\alpha}))$, model (28) can be approximated as follows:

$$\begin{bmatrix} \varkappa_{n+1} - \hat{\varkappa} \\ \gamma_{n+1} - \hat{\gamma} \end{bmatrix} \approx J(\hat{\varkappa}, \hat{\gamma}, \alpha_0) \begin{bmatrix} \varkappa_n - \hat{\varkappa} \\ \gamma_n - \hat{\gamma} \end{bmatrix} + C[\alpha - \alpha_0], \tag{29}$$

where

$$J(\hat{\varkappa}, \hat{\gamma}, \alpha_0) = \begin{bmatrix} \frac{\partial f(\hat{\varkappa}, \hat{\gamma}, \alpha_0)}{\partial \varkappa} & \frac{\partial f(\hat{\varkappa}, \hat{\gamma}, \alpha_0)}{\partial \gamma} \\ \frac{\partial g(\hat{\varkappa}, \hat{\gamma}, \alpha_0)}{\partial \varkappa} & \frac{\partial g(\hat{\varkappa}, \hat{\gamma}, \alpha_0)}{\partial \gamma} \end{bmatrix},$$

and

$$C = \begin{bmatrix} \frac{\partial f(\hat{\varkappa}, \hat{\gamma}, \alpha_0)}{\partial \alpha} \\ \frac{\partial g(\hat{\varkappa}, \hat{\gamma}, \alpha_0)}{\partial \alpha} \end{bmatrix} = \begin{bmatrix} -\frac{1}{4}h(\sqrt{\alpha^2+4\alpha} - \alpha)(-\alpha + \sqrt{\alpha^2+4\alpha} - 2) \\ 0 \end{bmatrix}.$$

It is easy to see that system (28) is controllable provided that the following matrix

$$\check{T} = [C : JC] = \begin{bmatrix} \frac{\partial f(\hat{\varkappa}, \hat{\gamma}, \alpha_0)}{\partial \alpha} & \frac{\partial f(\hat{\varkappa}, \hat{\gamma}, \alpha_0)}{\partial \varkappa} \cdot \frac{\partial f(\hat{\varkappa}, \hat{\gamma}, \alpha_0)}{\partial \alpha} \\ \frac{\partial g(\hat{\varkappa}, \hat{\gamma}, \alpha_0)}{\partial \alpha} & \frac{\partial g(\hat{\varkappa}, \hat{\gamma}, \alpha_0)}{\partial \varkappa} \cdot \frac{\partial g(\hat{\varkappa}, \hat{\gamma}, \alpha_0)}{\partial \alpha} \end{bmatrix}.$$

Since the matrix $\check{T}$ has a rank of 2 and $-\frac{1}{4}h(\sqrt{\alpha^2+4\alpha} - \alpha)(-\alpha + \sqrt{\alpha^2+4\alpha} - 2) \neq 0$, we proceed with the assumption that $[\alpha - \alpha_0] = -K \begin{bmatrix} \varkappa_n - \hat{\varkappa} \\ \gamma_n - \hat{\gamma} \end{bmatrix}$, where $K = \begin{bmatrix} \kappa_1 & \kappa_2 \end{bmatrix}$, then model (29) can be written as

$$\begin{bmatrix} \varkappa_{n+1} - \hat{\varkappa} \\ \gamma_{n+1} - \hat{\gamma} \end{bmatrix} \approx [J - CK] \begin{bmatrix} \varkappa_n - \hat{\varkappa} \\ \gamma_n - \hat{\gamma} \end{bmatrix}.$$

Moreover, the $p_1(\hat{\varkappa}, \hat{\gamma})$ is locally stable if and only if both eigenvalues of the matrix J - CK lie within an open unit disk. The matrix J - CK is given by the following expression:

$$J - CK = \begin{bmatrix} \Phi\kappa_1 + j_{11} & \Phi\kappa_2 + j_{12} \\ j_{21} & j_{22} \end{bmatrix},$$

where

$$j_{11} = 1 + h(\tfrac{1}{2}\alpha^2 - \tfrac{1}{2}\alpha\sqrt{\alpha^2 + 4\alpha}), \quad j_{12} = -\tfrac{1}{2}h(\sqrt{\alpha^2 + 4\alpha} - \alpha),$$

$$j_{21} = h(\sqrt{\alpha^2 + 4\alpha} - \alpha), \qquad j_{22} = 1 - h,$$

$$\Phi = \frac{1}{4}h(\sqrt{\alpha^2 + 4\alpha} - \alpha)(-\alpha + \sqrt{\alpha^2 + 4\alpha} - 2).$$

The characteristic equation of the matrix $J - CK$ is given by

$$\rho(\mathcal{R}) = \mathcal{R}^2 - (j_{11} + j_{22} + \Phi\kappa_1)\mathcal{R} + j_{22}(\Phi\kappa_1 + j_{11}) - j_{21}(\Phi\kappa_2 + j_{12}) = 0. \tag{30}$$

Let $\mathcal{R}_1$ and $\mathcal{R}_2$ represent the eigenvalues of the characteristic Equation (30). We then have:

$$\mathcal{R}_1 + \mathcal{R}_2 = j_{11} + j_{22} + \Phi\kappa_1, \tag{31}$$

and

$$\mathcal{R}_1\mathcal{R}_2 = j_{22}(\Phi\kappa_1 + j_{11}) - j_{21}(\Phi\kappa_2 + j_{12}). \tag{32}$$

Moreover, we take $\mathcal{R}_1 = \pm 1$ and $\mathcal{R}_1\mathcal{R}_2 = 1$. Thus, the lines of marginal stability of (31) and (32) are computed as follows:

$$\mathcal{L}_1 : j_{22}(\Phi\kappa_1 + j_{11}) - j_{21}(\Phi\kappa_2 + j_{12}) - 1 = 0. \tag{33}$$

Next, we suppose that $R_1 = 1$, then (32) and (31) yield that

$$\mathcal{L}_2 : j_{11} + j_{12}j_{21} + \Phi(j_{21}\kappa_2 + \kappa_1) + j_{22}(1 - \Phi\kappa_1 - j_{11}) - 1 = 0. \tag{34}$$

Finally, if $\mathcal{R}_1 = -1$ and using (31), then we obtain

$$\mathcal{L}_3 : j_{11} - j_{12}j_{21} + \Phi(\kappa_1 - j_{21}\kappa_2) + j_{22}(1 + \Phi\kappa_1 + j_{11}) + 1 = 0. \tag{35}$$

Therefore, the stability region of (28) is a triangular region bounded by $\mathcal{L}_1, \mathcal{L}_2$ and $\mathcal{L}_3$ in $\kappa_1\kappa_2$-plane.

5. Numerical Simulations

In this section, we present bifurcation diagrams, phase pictures, and maximum Lyapunov (ML in short) exponents of the model (4) to validate our theoretical findings and showcase the intricate dynamical behaviors through numerical simulations.

5.1. Period-Doubling Bifurcation

Example 1. ***Case 1.*** *We consider parameter h and examine the following subcases:*

(I) $\alpha = 4.04$. *In this case, we have a single positive fixed point. By performing calculations, we observe the PB of model (4) from* $p_1(\hat{\varkappa}, \hat{\gamma}) = (0.829631555, 0.688288520)$ *at* $h = 0.8874794$*, confirming Theorem 4. The values of* $\Psi_1 = -2.253699854$ *and* $\Psi_2 = 18.7591491$ *for* $(\alpha, h) \in F_{P_1}$ *are obtained. Figure 1a,b illustrate that* $p_1(\hat{\varkappa}, \hat{\gamma})$ *remains stable for* $0.87 \leq h < 0.8874794$ *but loses stability at the PB parameter value* $h = 0.8874794$*. Additionally, an orbit with a period of 2 is observed. The ML exponents corresponding to Figure 1a,b are depicted in Figure 1c.*

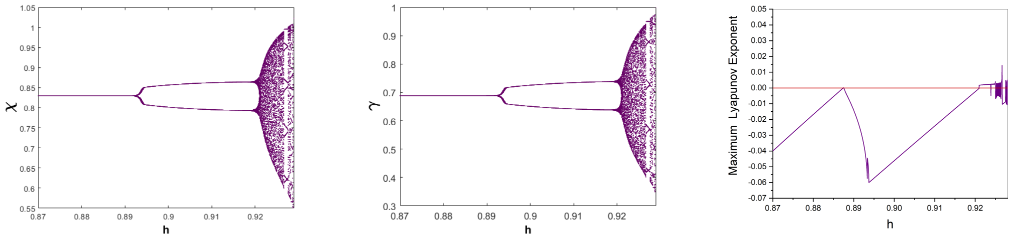

(**a**) (**b**) (**c**)

Figure 1. (**a**,**b**) Bifurcation diagram and (**c**) ML of model (4) for value of $\alpha = 4.04, h \in [0.87, 0.929]$.

(*II*) *For* $\alpha = 9$, *we computed the PB of model* (4) *and found that it occurred at* $p_1(\hat{\varkappa}, \hat{\gamma}) = (0.908326915, 0.82505776)$ *for* $h = 0.2519820562$ *with* $\Psi_1 = -7.937073099$, $\Psi_2 = 0.2377290476$ *and* $(\alpha, h) \in F_{P_1}$, *confirming Theorem 4. Observations from Figure 2a,b indicate that* $p_1(\hat{\varkappa}, \hat{\gamma})$ *remained stable for* $0.25 \leq h < 0.2519820562$ *but lost stability at the PB parameter value* $h = 0.2519820562$. *Additionally, orbits with periods of 2, 4, 8, and 16 were observed. The ML exponents corresponding to Figure 2a,b are shown in Figure 2c.*

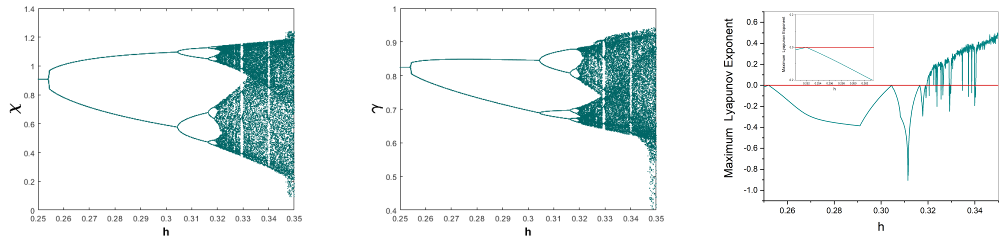

(**a**) (**b**) (**c**)

Figure 2. (**a**,**b**) Bifurcation diagram and (**c**) ML of model (4) for value of $\alpha = 9, h \in [0.25, 0.35]$.

Case 2. *We consider parameter* α *and examine the following subcases:*

$(I)'$ *At* $h = 0.8874794$, *we observe from Figure 3a,b, that* $p_1(\hat{\varkappa}, \hat{\gamma})$ *remains stable for* $4 \leq \alpha < 4.04$ *but loses stability at The PB parameter value* $\alpha = 4.04$. *Furthermore, there is an orbit with a period of 2. The ML exponents, corresponding to Figure 3a,b, are shown in Figure 3c.*

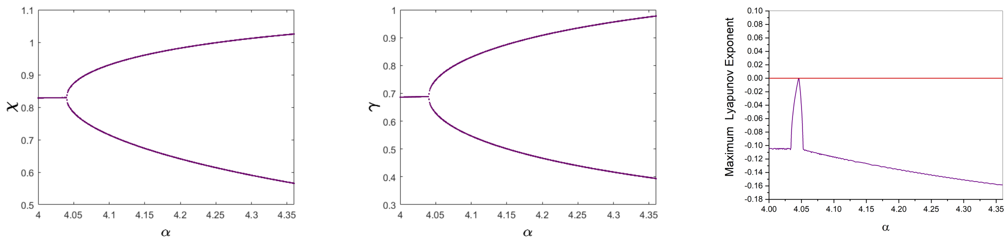

(**a**) (**b**) (**c**)

Figure 3. (**a**,**b**) Bifurcation diagram and (**c**) ML of model (4) for value of $h = 0.8874794, \alpha \in [4, 4.36]$.

$(II)'$ *At* $h = 0.2519820562$, *it can be observed from Figure 4a,b that* $p_1(\hat{\varkappa}, \hat{\gamma})$ *remains stable for the range* $8.5 \leq \alpha < 9$ *but loses its stability at the PB parameter value* $\alpha = 9$. *Furthermore, there are orbits with periods of 2, 4, 8, and 16. The ML exponents, corresponding to Figure 4a,b, are depicted in Figure 4c.*

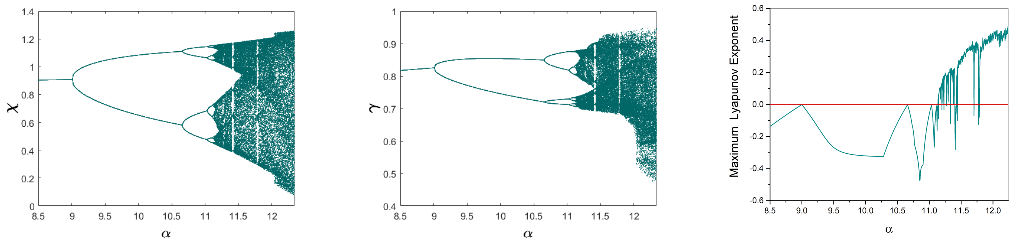

(**a**) (**b**) (**c**)

Figure 4. (**a**,**b**) Bifurcation diagram and (**c**) ML of model (4) for value of $h = 0.2519820562, \alpha \in [8.5, 12.34]$.

5.2. Neimark–Sacker Bifurcation

Example 2. ***Case 3.*** *We consider parameter h and examine the following subcases:*

(I) *For α = 0.6, the NB of Model (4) occurs, revealing the fixed point* $p_1(\hat{\varkappa}, \hat{\gamma}) = (0.5306623865, 0.2816025681)$ *at h = 1.495455526. This fixed point satisfies* $\xi = -1.033549625$ *and* $(\alpha, h) \in N_{p_1}$*, confirming the validity of Theorem 5. Observing Figure 5a,b, it can be seen that* $p_1(\hat{\varkappa}, \hat{\gamma})$ *remains stable for* $0 < h < 1.495455526$ *but loses stability at the NB parameter value h = 1.495455526. The ML exponents, shown in Figure 5c, are correlated with Figure 5a,b. Additionally, Figure 6 displays the phase pictures associated with Figure 5a,b.*

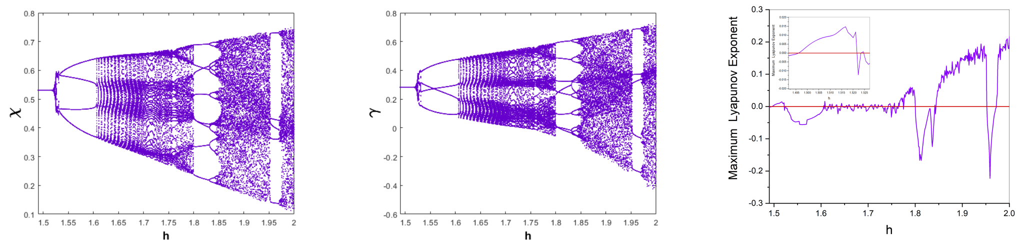

(**a**) (**b**) (**c**)

Figure 5. (**a**,**b**) Bifurcation diagram and (**c**) ML of model (4) for value of $\alpha = 0.6, h \in [1.49, 2]$.

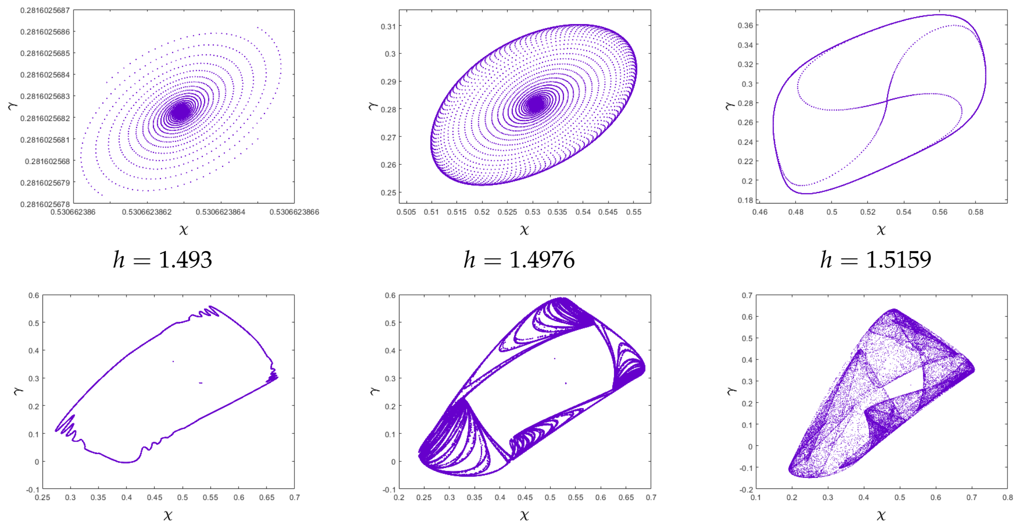

$h = 1.493$ $h = 1.4976$ $h = 1.5159$

$h = 1.746$ $h = 1.795$ $h = 1.865$

Figure 6. *Cont.*

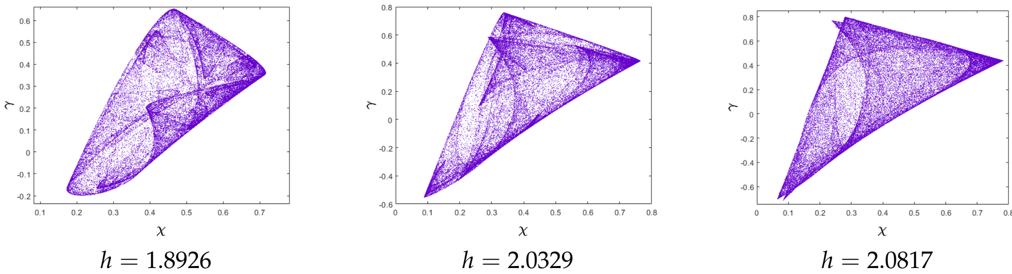

Figure 6. The phase pictures associated with Figure 5a,b.

(II) *For $\alpha = 2.1$, we computed the NB of Model (4), which resulted in the fixed point $p_1(\hat{\varkappa}, \hat{\gamma}) = (0.739553017, 0.546938664)$ at $h = 0.9645336217$. This fixed point satisfies $\xi = -0.0983919023$ and $(\alpha, h) \in N_{P_1}$, illustrating the validity of Theorem 5. By examining Figure 7a,b, we observe that $p_1(\hat{\varkappa}, \hat{\gamma})$ remains stable for $0 < h < 0.9645336217$ but loses stability at the NB parameter value $h = 0.9645336217$. The ML exponents, shown in Figure 7c, are correlated with Figure 7a,b. Furthermore, Figure 8 displays the phase pictures associated with Figure 7a,b.*

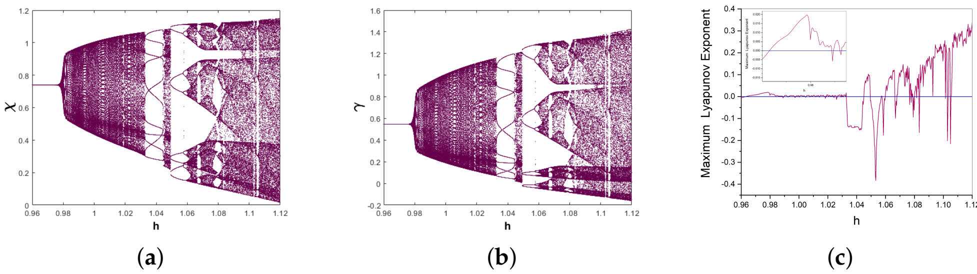

Figure 7. (**a**,**b**) Bifurcation diagram and (**c**) ML of model (4) for value of $\alpha = 2.1, h \in [0.96, 1.12]$.

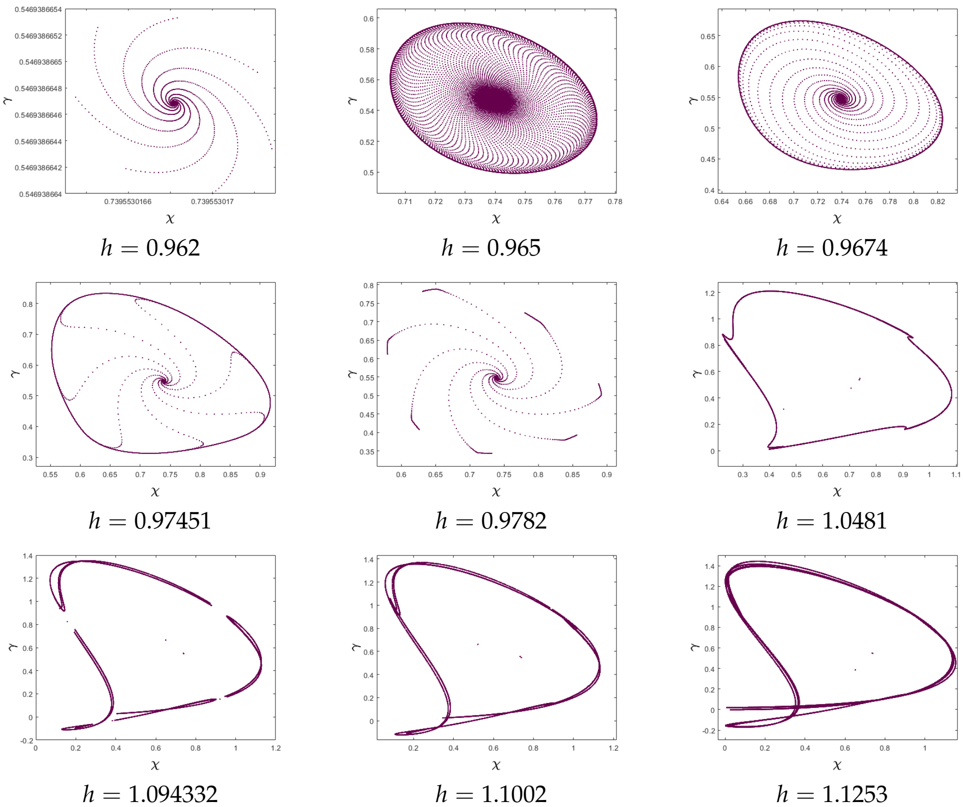

Figure 8. The phase pictures associated with Figure 7a,b.

Case 4. *We consider parameter α and examine the following subcases:*

$(I)'$ *Let $h = 0.9336269198$. It is observed from Figure 9a,b that $p_1(\hat{\varkappa}, \hat{\gamma})$ remains stable for the parameter range of $2.6 \leq \alpha < 2.85$. However, it loses stability at the NB parameter value of $2.85 \leq \alpha < 2.8634708$. then it suddenly transitions to a steady state. The ML exponents, depicted in Figure 9c, confirm this behavior. Additionally, Figure 9d depicts a LA for $\alpha \in [2.6, 2.91]$. Furthermore, Figure 10 displays the phase pictures corresponding to Figure 9a,b.*

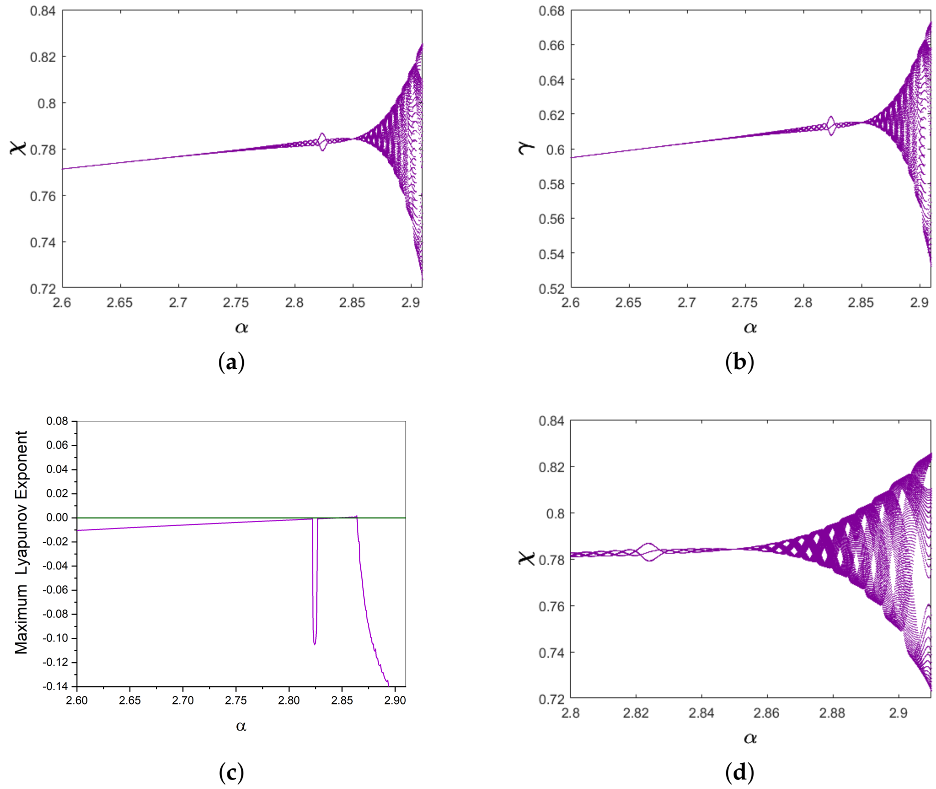

Figure 9. (**a**,**b**) Bifurcation diagram and (**c**) ML of model (4) for value of $h = 0.9336269198$, $\alpha \in [2.6, 2.91]$ and (**d**) LA for $\alpha \in [2.8, 2.91]$.

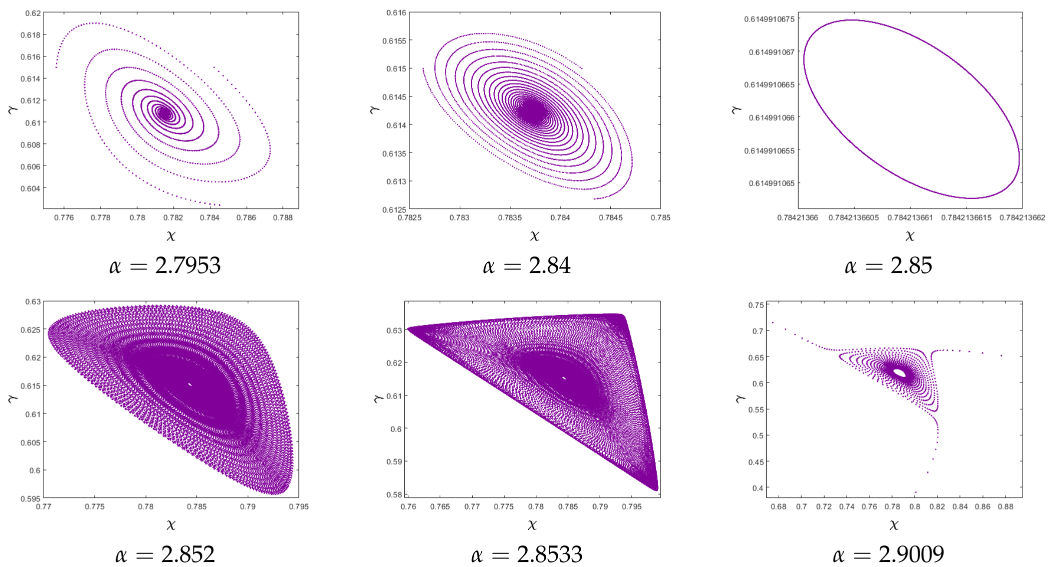

Figure 10. The phase pictures associated with Figure 9a,b.

$(II)'$ *If h = 1.495455526, we observe from Figure 11a,b that* $p_1(\hat{\varkappa}, \hat{\gamma})$ *is stable within the parameter range of* $0.5 \leq \alpha < 0.6$*. However, it loses stability at the NB parameter value α = 0.6. The ML exponents, depicted in Figure 11c, are related to Figure 11a,b.*

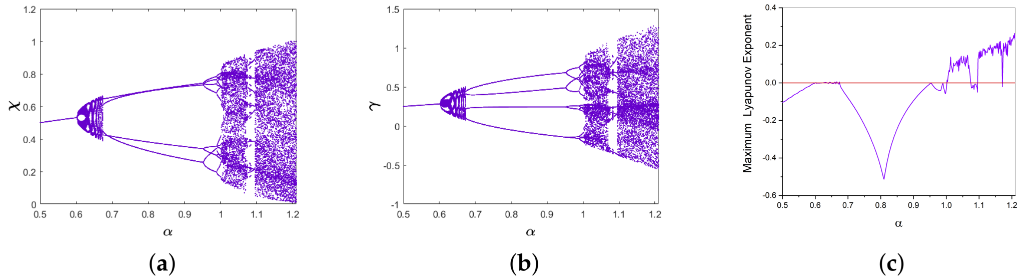

Figure 11. (**a**,**b**) Bifurcation diagram and (**c**) ML of model (4) for value of $h = 1.495455526$, $\alpha \in [0.5, 1.21]$.

$(III)'$ *If* $h = 0.9645336217$*, it is observed from Figure 12a,b that* $p_1(\hat{\varkappa}, \hat{\gamma})$ *remains stable for the parameter range of* $1.98 \leq \alpha < 2.02061$*. However, it loses stability at the NP parameter value* $\alpha = 2.02061$*. Next, we find that the dynamics of the Lorenz model reach their highest chaotic value when* $\alpha = 2.666659$*, and then it suddenly transitions to a steady state. The ML exponents, depicted in Figure 12c, confirm this behavior.*

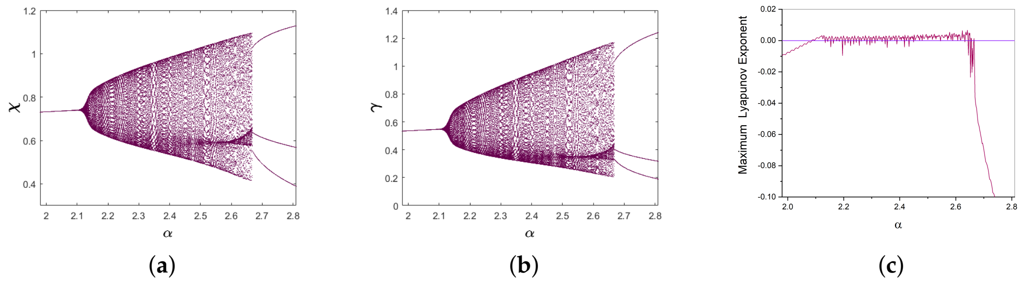

Figure 12. (**a**,**b**) Bifurcation diagram and (**c**) ML of model (4) for value of $h = 0.9645336217$, $\alpha \in [1.98, 2.81]$.

5.3. Control of Chaos

To study the chaos control for model (4), we apply the OGY method with parameters α = 0.45 and h = 1.782443101. Model (4) has an equilibrium point $p_1(\hat{\varkappa}, \hat{\gamma}) = (0.482548585, 0.2328531368)$, which is unstable. We consider $\alpha_0 = 0.45$ as the nominal value. Therefore, the controlled model is formulated as follows:

$$\begin{aligned} \varkappa_{n+1} &= (1 + (\alpha_0 - \kappa_1(\varkappa_n - \hat{\varkappa}) - \kappa_2(\gamma_n - \hat{\gamma}))h)\varkappa_n \\ &\quad - h\varkappa_n\gamma_n - (\alpha_0 - \kappa_1(\varkappa_n - \hat{\varkappa}) - \kappa_2(\gamma_n - \hat{\gamma}))h\varkappa_n^2, \\ \gamma_{n+1} &= (1-h)\gamma_n + h\varkappa_n^2. \end{aligned} \tag{36}$$

Let $\mathcal{K}=\begin{bmatrix} \kappa_1 & \kappa_2 \end{bmatrix}$ be the gain matrix, and $p_1(\hat{\varkappa}, \hat{\gamma}) = (0.4825485850, 0.2328531368)$ be the unstable equilibrium point of model (4). Additionally, we obtain the following:

$$J = \begin{bmatrix} 0.6129480718 & -0.8601153962 \\ 1.720230792 & -0.782443101 \end{bmatrix},$$

$$C = \begin{bmatrix} 0.4450679288 \\ 0 \end{bmatrix},$$

and

$$\mathcal{T} = [C : JC] = \begin{bmatrix} 0.4450679288 & 0.2728035288 \\ 0 & 0.7656195557 \end{bmatrix}.$$

Then, it is easy to verify that the rank of $\mathcal{T}$ is 2. Therefore, the controlled model (36) is controllable. Moreover, the Jacobian matrix $J - CK$ of the controlled model (36) is given by

$$J - CK = \begin{bmatrix} 0.6129480718 - 0.4450679288\kappa_1 & -0.8601153962 - 0.4450679288\kappa_2 \\ 1.720230792 & -0.782443101 \end{bmatrix}. \quad (37)$$

Then, the characteristic equation of (37) is given by

$$\begin{aligned} \boldsymbol{\kappa}(\mathcal{R}) &= \mathcal{R}^2 + (0.169495029 + 0.4450679288\kappa_1)\mathcal{R} + 1 \\ &\quad +0.7656195559\kappa_2 + 0.3482403304\kappa_1. \end{aligned} \quad (38)$$

Then, the roots of Equation (38) lie within a unit disk $|\mathcal{R}| < 1$ if the following conditions are satisfied:

$$\begin{aligned} 0 &< 0.4548477474\kappa_1 + \kappa_2, \\ 4.112866492 &> \kappa_1 \geq -0.3808295724, 2.390880636 \\ +\kappa_2 &> 0.1264695992\kappa_1, \end{aligned}$$

or

$$-0.3808295724 > \kappa_1 > -4.874525637, 2.833646309 + 1.036165094\kappa_1 > -\kappa_2.$$

In this case, the lines of subaltern stability are given by

$$\mathcal{L}_1 : 0.3482403304\kappa_1 + 0.7656195559\kappa_2 = 0,$$

$$\mathcal{L}_2 : 1.830504971 + 0.7656195559\kappa_2 = 0.0968275984\kappa_1,$$

and

$$\mathcal{L}_3 : 0.7933082592\kappa_1 + 0.7656195559\kappa_2 + 2.169495029 = 0.$$

The stable triangular region, delineated by the sub-lines $\mathcal{L}_1$, $\mathcal{L}_2$ and $\mathcal{L}_3$ in the controlled model (36) is depicted in Figure 13a. Moving forward, by setting $\kappa_1 = 1$, we find that the fixed point of the controlled model (36) is locally stable if and only if $-2.264411037 < \kappa_2 < -0.4548477474$. To further explore the dynamics, we choose $\kappa_1 = 1$ and $\kappa_2 \in [-3.5, 1]$, and present the bifurcation diagrams of the controlled model (36) in Figure 13b. In addition, we provide examples of the phase of chaos control bifurcation [28]. Specifically, we consider κ_2 as a variable and illustrate the behavior of $\varkappa_n$ for $\kappa_2 \in [-3.5, 1]$. Figure 14 showcases various values of κ_1 as indicated below:

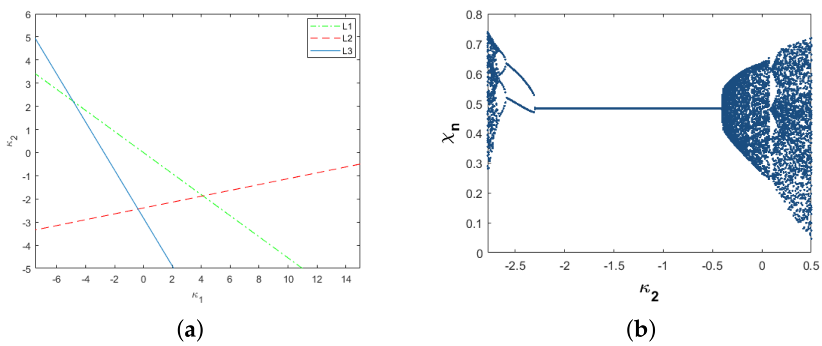

Figure 13. (**a**) The region of stability for the controlled model (36). (**b**) Diagrams of bifurcation for the controlled model (36) with $\kappa_1 = 1$, $p_1(\hat{\varkappa}, \hat{\gamma}) = (0.482548585, 0.2328531368)$ and $\kappa_2 \in [-3.5, 1]$.

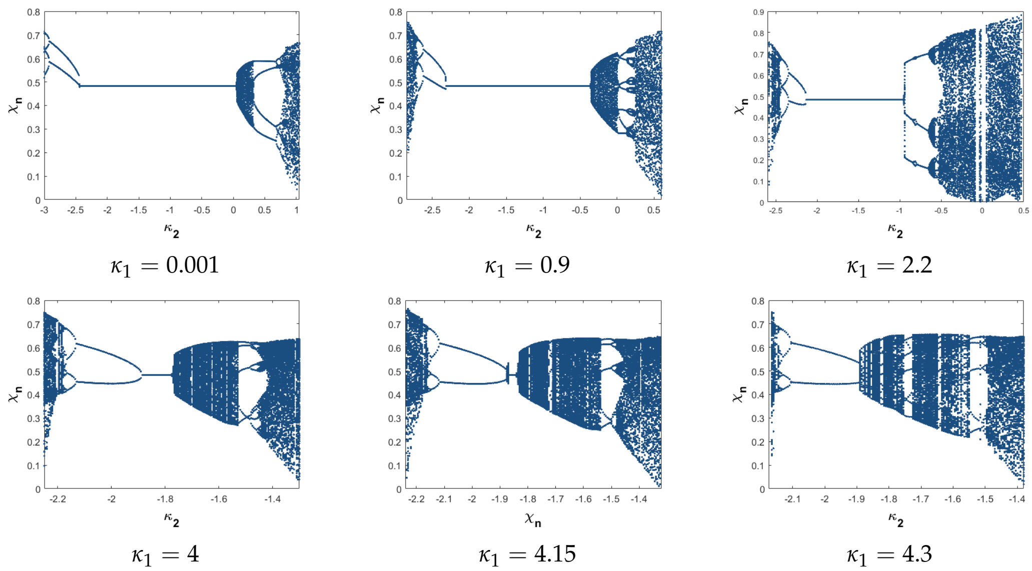

Figure 14. The Phase of Chaos of the controlled model (36).

6. Conclusions

This study investigates the bifurcation behavior and chaos control in a two-dimensional modified reduced Lorenz model. We examine the existence and uniqueness of a positive steady state within the model. According to our theoretical study, the model (4) undergoes pitchfork bifurcation, period-doubling bifurcation, and Neimark–Sacker bifurcation. Our theoretical approach is supported by numerical simulations, which include bifurcation diagrams, phase pictures, and maximum Lyapunov exponents for all model parameters (4). These findings reveal interesting dynamic behaviors, such as stationary cycles and chaotic attractors, confirming our theoretical analysis. The results contribute to a comprehensive understanding of the modified Lorenz Reduction Model and its potential applications in information security, the basin of attraction identification, and adaptive and global synchronization. We employ a chaos control strategy to manage the chaotic behavior of the model (4), and its effectiveness is demonstrated through numerical simulations. Finally, we present examples of chaos control bifurcation phases.

Author Contributions: Conceptualization, M.O.A.-K., G.A. and E.M.E.; methodology, M.O.A.-K., G.A., A.-E.A.E., H.A.E.-M. and E.M.E.; software, M.O.A.-K., G.A. and E.M.E.; validation, M.O.A.-K., G.A. and A.-E.A.E.; formal analysis, M.O.A.-K., G.A. and H.A.E.-M.; investigation, M.O.A.-K., G.A. and E.M.E.; resources, M.O.A.-K., G.A. and E.M.E.; data curation, M.O.A.-K., G.A. and E.M.E.; writing—original draft preparation; M.O.A.-K., G.A. and E.M.E.; writing—review and editing, M.O.A.-K., G.A., A.-E.A.E. and E.M.E.; visualization, M.O.A.-K., G.A. and A.-E.A.E.; supervision, E.M.E., H.A.E.-M. and A.-E.A.E. All authors have read and agreed to the published version of this manuscript.

Funding: Princess Nourah bint Abdulrahman University Researchers Supporting Project Number (PNURSP2024R45), Princess Nourah bint Abdulrahman University, Riyadh, Saudi Arabia.

Data Availability Statement: Data are contained within the article.

Conflicts of Interest: The authors declare that they have no conflicts of interest regarding the publication of this article.

References

1. Wang, M.; Wang, X.; Zhang, Y.; Gao, Z. A novel chaotic encryption scheme based on image segmentation and multiple diffusion models. *Opt. Laser Technol.* **2018**, *108*, 558–573. [CrossRef]
2. Yang, Y.G.; Guan, B.W.; Li, J.; Li, D.; Zhou, Y.H.; Shi, W.M. Image compression-encryption scheme based on fractional order hyper-chaotic systems combined with 2D compressed sensing and DNA encoding. *Opt. Laser Technol.* **2019**, *119*, 105661. [CrossRef]

3. Elsadany, A.A.; Yousef, A.M.; Elsonbaty, A. Further analytical bifurcation analysis and applications of coupled logistic maps. *Appl. Math. Comput.* **2018**, *338*, 314–336. [CrossRef]
4. Henon, M. A two-dimensonal mapping with a strange attractor. *Commun. Math. Phys.* **1976**, *50*, 376–392. [CrossRef]
5. Lorenz, E.N. Deterministic nonperiodic flow. *J. Atmos. Sci.* **1963**, *20*, 130–141. [CrossRef]
6. Annaby, M.H.; Rushdi, M.A.; Nehary, E.A. Color image encryption using random transforms, phase retrieval, chaotic maps, and diffusion. *Opt. Lasers Eng.* **2018**, *103*, 9–23. [CrossRef]
7. Mliki, E.; Hasanzadeh, N.; Nazarimehr, F.; Akgul, A.; Boubaker, O.; Jafari, S. Some new chaotic maps with application in stochastic. In *Recent Advances in Chaotic Systems and Synchronization*; Academic Press: Cambridge, MA, USA, 2019; pp. 165–185.
8. Ramadoss, J.; Natiq, H.; Nazarimehr, F.; He, S.; Rajagopal, K.; Jafari, S. A novel chaotic map with a shifting parameter and stair-like bifurcation diagram: Dynamical analysis and multistability. *Phys. Scr.* **2023**, *98*, 025212. [CrossRef]
9. Lorenz, E.N. Computational chaos-a prelude to computational instability. *Phys. D Nonlinear Phenom.* **1989**, *35*, 299–317. [CrossRef]
10. Frouzakis, C.E.; Kevrekidis, I.G.; Peckham, B.B. A route to computational chaos revisited: Noninvertibility and the breakup of an invariant circle. *Phys. D Nonlinear Phenom.* **2003**, *177*, 101–121. [CrossRef]
11. Elabbasy, E.M.; Elsadany, A.A.; Zhang, Y. Bifurcation analysis and chaos in a discrete reduced Lorenz system. *Appl. Math. Comput.* **2014**, *228*, 184–194. [CrossRef]
12. Zhao, J.; Yan, Y. Stability and bifurcation analysis of a discrete predator–prey system with modified Holling–Tanner functional response. *Adv. Differ. Equ.* **2018**, *2018*, 402. [CrossRef]
13. Al-Kaff, M.O.; El-Metwally, H.A.; Elabbasy, E.M.; Elsadany, A.E.A. Dynamic Behaviors in a Discrete Model for Predator–Prey Interactions Involving Hibernating Vertebrates. *Int. J. Bifurc. Chaos* **2023**, *33*, 2350182. [CrossRef]
14. Zhang, L.; Zhang, C.; He, Z. Codimension-one and codimension-two bifurcations of a discrete predator–prey system with strong Allee effect. *Math. Comput. Simul.* **2019**, *162*, 155–178. [CrossRef]
15. Streipert, S.H.; Wolkowicz, G.S.; Bohner, M. Derivation and analysis of a discrete predator–prey model. *Bull. Math. Biol.* **2022**, *84*, 67. [CrossRef] [PubMed]
16. Tassaddiq, A.; Shabbir, M.S.; Din, Q.; Naaz, H. Discretization, bifurcation, and control for a class of predator-prey interactions. *Fractal Fract.* **2022**, *6*, 31. [CrossRef]
17. Elettreby, M.F.; Nabil, T.; Khawagi, A. Stability and Bifurcation Analysis of a Discrete Predator-Prey Model with Mixed Holling Interaction. *Cmes-Comput. Model. Eng. Sci.* **2020**, *122*, 907–922. [CrossRef]
18. Khan, A.Q.; Bukhari, S.A.H.; Almatrafi, M.B. Global dynamics, Neimark–Sacker bifurcation and hybrid control in a Leslie's prey-predator model. *Alex. Eng. J.* **2022**, *61*, 11391–11404. [CrossRef]
19. Lei, C., Han, X.; Wang, W. Bifurcation analysis and chaos control of a discrete-time prey-predator model with fear factor. *Math. Biosci. Eng.* **2022**, *19*, 6659–6679. [CrossRef] [PubMed]
20. Askar, S.S.; Karawia, A.A.; Al-Khedhairi, A.; Al-Ammar, F.S. An algorithm of image encryption using logistic and two-dimensional chaotic economic maps. *Entropy* **2019**, *21*, 44. [CrossRef]
21. Qian, X.; Yang, Q.; Li, Q.; Liu, Q.; Wu, Y.; Wang, W. A novel color image encryption algorithm based on three-dimensional chaotic maps and reconstruction techniques. *IEEE Access* **2021**, *9*, 61334–61345. [CrossRef]
22. Zhu, S.; Zhu, C. Plaintext-related image encryption algorithm based on block structure and five-dimensional chaotic map. *IEEE Access* **2019**, *7*, 147106–147118. [CrossRef]
23. Liu, X.; Xiao, D. Complex dynamic behaviors of a discrete-time predator–prey system. *Chaos Solitons Fractals* **2007**, *32*, 80–94. [CrossRef]
24. Wiggins, S. Hamiltonian Vector Fields. In *Introduction to Applied Nonlinear Dynamical Systems and Chaos*; Springer: Cham, Switzerland, 2003; pp. 197–230.
25. Carr, J. *Applications of Centre Manifold Theory*; Springer Science & Business Media: Berlin/Heidelberg, Germany, 2012.
26. Robinson, C. *Dynamical Systems: Stability, Symbolic Dynamics, and Chaos*; CRC Press: Boca Raton, FL, USA, 1998.
27. Ott, E.; Grebogi, C.; Yorke, J. A. Controlling chaos. *Phys. Rev. Lett.* **1990**, *64*, 1196–1199. [CrossRef] [PubMed]
28. Al-Kaff, M.O.; El-Metwally, H.A.; Elabbasy, E.M. Qualitative analysis and phase of chaos control of the predator-prey model with Holling type-III. *Sci. Rep.* **2022**, *12*, 20111. [CrossRef] [PubMed]